

The bow shock and jet in L483

J.V. Buckle, J. Hatchell, and G.A. Fuller

Department of Physics, UMIST, P.O. Box 88, Manchester M60 1QD, UK

Received 27 January 1999 / Accepted 25 May 1999

Abstract. The physical parameters of jets are still poorly understood. Here we present long slit spectra of the molecular hydrogen emission from the jet powered by the young stellar object in L483, from which we obtain details of the jet structure and shock velocities. The jet has a knotty structure, and, in addition, weaker emission is seen between the knots, so that emission is observed along the full length of the jet. The H₂ emission from the bright bow shock at the end of the jet has an excitation temperature of 2200 K, and is consistent with a bow C-shock of speed 40–45 km s⁻¹. Lower speed J-shocks, which could also match the H₂ emission, are ruled out by a lower limit on the shock speed provided by an analysis of the CO emission from the outflow. Assuming a jet velocity of ~ 200 km s⁻¹, this shock velocity indicates that the jet from L483 has a density of about 10 times less than the medium into which it is propagating. The H₂ knots are possibly due to jet instabilities, or could be indicative of episodic activity. Emission from between the knots could be indicative of a partially molecular jet, entrainment in a mixing layer, or unresolved sub-knots. These possibilities, and how they impact on outflow models, are discussed.

Key words: stars: formation – ISM: individual objects: L483 – ISM: jets and outflows – ISM: kinematics and dynamics – ISM: molecules

1. Introduction

Outflows are an essential part of star formation and cloud evolution. They remove excess angular momentum from the protostellar system, and can also contribute to turbulent support for the cloud. However, there is little consensus on the dynamics of the jets and outflows. Observations suggest that the outflows consist of jet-accelerated molecular gas, thought to be powered by the accretion process (Königl 1995). The outflows generally have two components, a highly collimated high velocity jet, and a more poorly collimated low velocity outflow, both of which are usually bipolar.

As the material in the jet impacts with the surrounding ambient medium, shocks form, which allow the kinetic energy of high velocity material to be dissipated and radiated away. Ambient material is swept up around the jet, in an entrainment process,

forming the molecular outflow. Episodic outflow activity, or jet instabilities, can lead to a series of knots in the jet.

Jets have been observed in vibrational molecular hydrogen lines, which are thought to be emitted in cooling regions behind shocks. The excitation pattern in molecular hydrogen is indicative of the type of excitation mechanism. Emission in vibrational transitions of molecular hydrogen is only significant for temperatures > 1000 K, and since the cooling timescales are short compared to the dynamical timescales of outflows, molecular hydrogen emission traces non dissociative shocks, or regions heated by some other energetic means such as UV excitation (Fernandes & Brand 1995; Hora & Latter 1994).

The Lynds 483 dark cloud contains IRAS 18148-0440, a deeply embedded, very young source, with a luminosity of < 14 L_☉ (Fuller et al. 1995). It is assumed to be at a distance of 200 pc, and has an age, estimated from the outflow velocity, and including a correction for inclination angle, of 4 × 10³ yrs. The bolometric temperature (Myers & Ladd 1993), calculated from the spectral energy distribution, is 57 K, which reinforces the young age estimate.

Dense gas surrounds the source, which has a low velocity bipolar molecular outflow, and a collimated jet which displays a knotty structure. The outflow is inclined close to the plane of the sky, and has been observed in CO J=2→1 (Hatchell et al. 1999; Parker et al. 1991), 3→2 (Fuller et al. 1995) and 4→3 (Hatchell et al. 1999) transitions. There are two spatially separated lobes, extending east and west of the source, with an aspect ratio of ≈ 5:1. The lobes extend over 22 × 10³ AU, with a maximum velocity of ±5 km s⁻¹, and a temperature of at least 20 K to 60 K (Hatchell et al. 1999), consistent with the predictions for a jet-driven outflow model (Masson & Chernin 1993). The jet is visible in the blue-shifted lobe, and extends over 12 × 10³ AU. It has been mapped in H₂, which shows a knot of emission connected by a weaker, jet-like structure to the embedded source (Fuller et al. 1995).

In this paper, we present the results of longslit spectroscopy of the jet/outflow system in L483. Although H₂ spectroscopy has been carried out on a number of young sources (e.g. Fernandes & Brand 1995; Wright et al. 1996), our study is important, as it is the first to target a Class 0 source. The dynamics of these less evolved jets may be simpler to understand than their more complex evolved counterparts. In Sect. 2, we describe the observations and data reduction. In Sect. 3 we present the results,

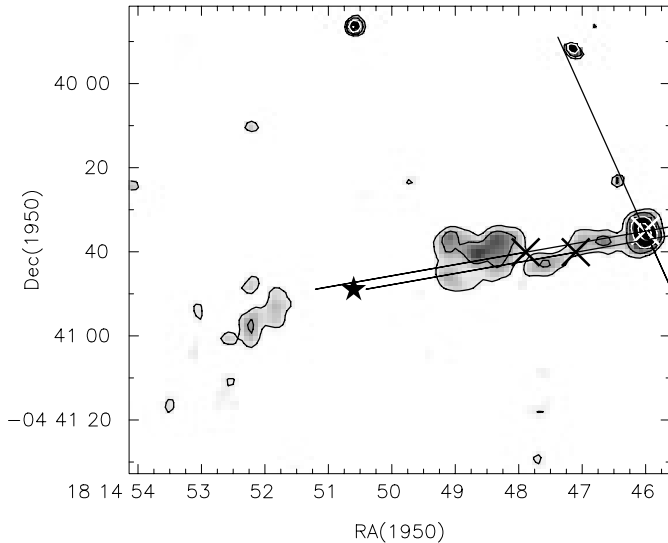


Fig. 1. Position of the CGS4 slits relative to the H_2 emission. The image of H_2 emission is formed from the difference between $2.12 \mu\text{m}$ and $2.22 \mu\text{m}$ images (Fuller et al. 1995). A star marks the IRAS source, and crosses mark the slit centres. Slit 1 runs almost perpendicular to the outflow axis, through the head of the jet. Slits 2 and 3 are parallel to each other, with slit 2 being $2''$ north of slit 3.

and in Sect. 4 we analyse the resulting temperature, density and spatial structure. In Sect. 5 we look at the emission from the peaks in the light of recent shock models, and in Sect. 6 we discuss the processes underlying the continuous emission. Finally, in Sect. 7 we summarise our findings.

2. Observations and data reduction

The observations were obtained at the 3.8 m UKIRT telescope on Mauna Kea, Hawaii over two nights in May/June 1997. The longslit capability of the CGS4 cooled grating spectrometer was used with the 150 mm focal length camera, and 75 l/mm grating, to measure H_2 emission in the K-band in the outflow of L483, giving a wavelength coverage of $1.85 \mu\text{m}$ to $2.52 \mu\text{m}$. The slit size is approximately $90 \times 1.2 \text{ arcsec}^2$, and the configuration gives a spectral resolution of $0.003 \mu\text{m}$ at $2.2 \mu\text{m}$. The seeing was $1.8''$, obtained from the FWHM size of a standard star.

The slit was placed in three different positions (Fig. 1) through the outflow, chosen to cut the bright jet head in two directions and also cover the more extended emission between the jet head and the source. The slits were positioned using offsets from a nearby star. The positions from Fig. 1 are correct to within $\leq 1''$. The details of the observations are given in Table 1. Towards the source, there is a nebulosity which has been imaged in the K band, and slit 2, which is along the jet axis, also passes through this bright nebulosity near the source.

The observations were taken in object-sky pairs. The integration times gave an RMS noise in the spectra of $\sim 9 \times 10^{-15} \text{ erg s}^{-1} \text{ cm}^{-2} \mu\text{m}^{-1}$. The data were reduced using the CGS4 data reduction package. Wavelength calibration was undertaken using the OH sky lines from the raw spectra. The RMS

uncertainty in the wavelength scale corresponds to $\approx 45 \text{ km s}^{-1}$. We didn't detect any velocity shift $> 3 \times 45 \text{ km s}^{-1}$.

For each slit position, every object observation was flat-fielded and sky-subtracted, removing the dark current, and then added together to form a single group. The observations were taken in non-destructive read mode, so removing the need to subtract a bias level. Flux calibration was provided by dividing the reduced spectra by the spectra of a standard star. This also corrected for atmospheric absorption lines. Standard stars were observed at the start and end of each set of observations. The standard stars used were BS7288, with a K magnitude of 6.13 (Catalog of IR Observations), and BS6830, whose K magnitude was taken to be 6.1 (Koornneef 1983). The uncertainty is estimated to be 4% in the line fluxes. However, given the seeing and the slit width, it is unlikely that the observations contain all of the flux from the standard star, as the star is not exactly centred on the slit. Therefore, the calibration method provides a lower limit on the stellar flux, and therefore an upper limit on the line intensities. Since the analysis is based on line ratios, this does not unduly influence the conclusions, except that the derived column densities are upper limits.

3. Results

The data were analysed using the Figaro packages Twodspec and Longslit. Spectra at three positions along the jet are shown in Fig. 2. The spectra from all positions along the jet are dominated by the $v=1-0$ lines, particularly the S(1), S(3) and Q lines. Also present in the spectra are weaker lines from the $v=2-1$ and $v=3-2$ bands. The emission from lines with $v>1$ is weak compared to the $1-0$ S(1) lines. The appearance of apparent absorption lines is not significant, as these are due to poorly subtracted atmospheric lines. The apparent weak emission feature close to $2.16 \mu\text{m}$ in the spectrum of the nebula (Fig. 2c) is probably due to Brackett gamma absorption in the standard stars.

A comparison of Figs. 2a and 2b shows that the lines are an order of magnitude brighter at the head of the jet than in the body of the jet. The general pattern of the emission lines is, however, the same. The $v=1-0$ lines are visible at all positions along the jet. The $v=2-1$ lines and $v=3-2$ lines can clearly be seen at the head of the jet, but as the intensity of the lines falls along the jet, these higher excitation level lines fall below the RMS noise in the spectra. The $v=2-1$ and $v=3-2$ lines are detectable at points along the jet where the emission is stronger, but at positions where the intensity of the $v=1-0$ lines falls by 2 orders of magnitude, the higher excitation lines are not detectable above the RMS noise.

Near the source, the jet is coincident with a bright nebula, which is seen in the K-band continuum. The K-band continuum can be explained as light from the central source scattered from the edge of the cavity excavated by the outflow. Fig. 2c shows H_2 lines superimposed on this continuum. The continuum is rather red in colour, rising towards longer wavelengths, indicating that the source is indeed young and deeply embedded. As scattering would be expected to make a spectrum more blue, the light being scattered by the cavity walls must be very red, indicating that

Table 1. CGS4 Observations

Slit No.	Description	PA °	Slit Centre RA (1950) DEC (1950)	UT Date	Integration Time min
Slit 1	Across bow shock	+24	18 14 46.01 −04 40 35.0	31-05-97	24
Slit 2	Along jet axis	−70	18 14 48.05 −04 40 41.3	01-06-97	72
Slit 3	Offset 11.8'' west, 2'' south of Slit 2	−70		01-06-97	60

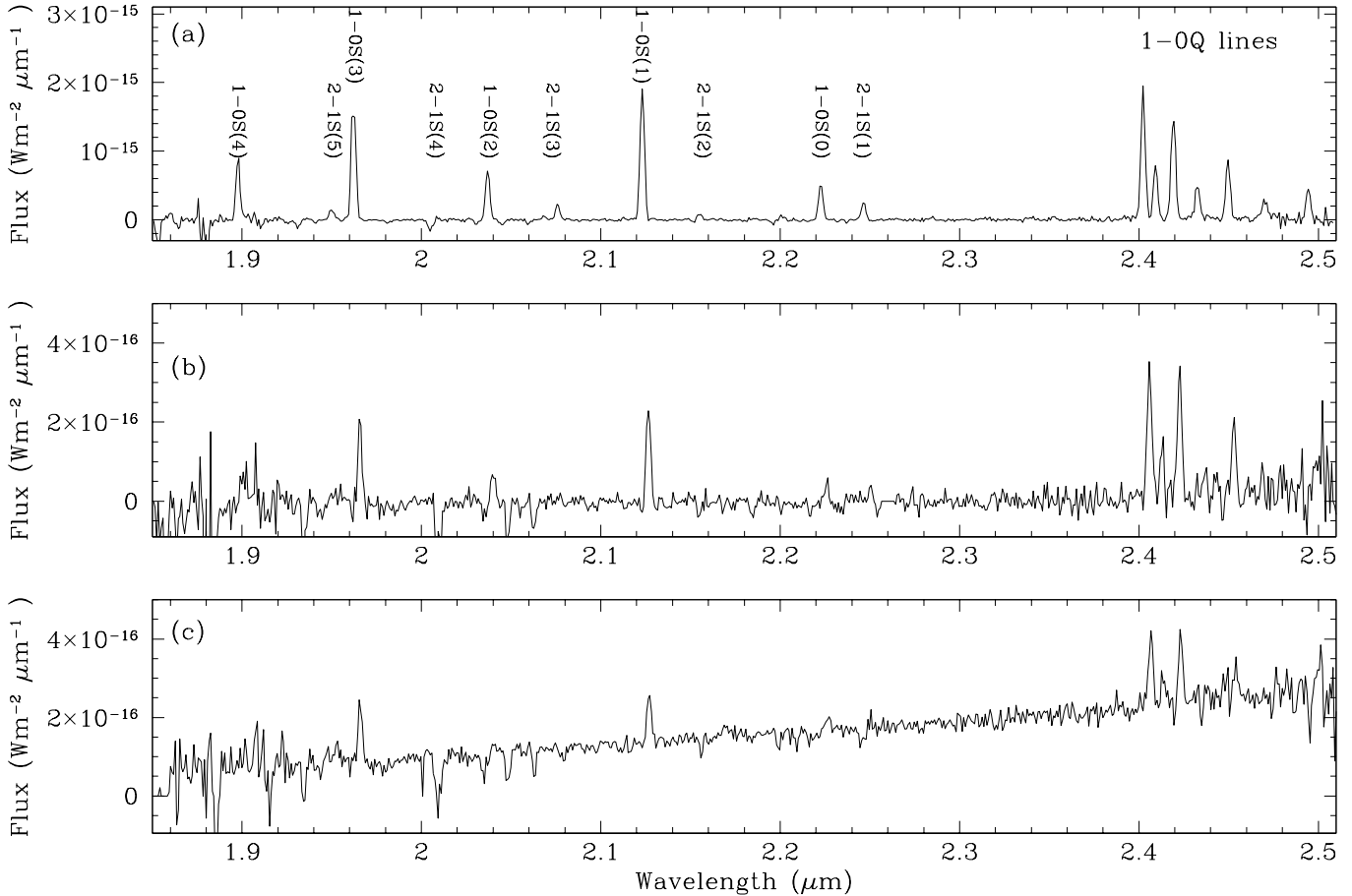


Fig. 2a–c. H₂ emission lines from: **a** The head of the jet (Slit 1), taken across row 19 where the emission from the jet head peaks. The strongest H₂ lines are marked. **b** The main body of the jet (Slit 2), taken across row 32. **c** The jet near the source (Slit 2), taken across row 64.

there is dust between the source and the scattering location, or that the source has an intrinsically red spectrum.

The extinction can be calculated from the ratio of the $\frac{1-0S(1)}{1-0Q(3)}$ lines, which originate from the same upper state (Fernandes & Brand 1995). The observed ratio of the line intensities towards the nebula gives $A_{2.2}=3.8$ mag at this position, which corresponds to an extinction of ~ 38 mag at visual wavelengths, assuming that the extinction scales as the wavelength to the power -1.7 . Towards both the jet and jet head, the extinction is about 3 times less.

Fig. 3a shows a cut along the length of the jet in the 1–0S(1) line at $2.12 \mu\text{m}$. Fig. 3b shows the same cut in a line free part of the spectrum. These figures show that the jet has knots of brighter emission (labelled Peaks 1, 2 and 3) between the head

of the jet, at row 20, and the rise in the continuum at row 60. These peaks are coincident with the knots of H₂ emission seen in Fig. 1. The approximate distances between the peaks, starting from the head of the jet are 2400 AU to peak 1, 1000 AU to peak 2, and 3400 AU to peak 3. The off axis slit (slit 3) shows a fourth emission peak near the nebulosity, which is between the peaks labelled 2 and 3 in slit 2. This emission peak lies between the two knots of emission shown in Fig. 1, just below the central cross of slit 1. As can be seen from Fig. 3, H₂ emission is also seen between the emission peaks. Two of these positions have been labelled as Troughs 1 and 2. This is inter-clump emission detected in the other strong H₂ lines, and in the off-axis slit. The emission from the troughs, between the peaks, is an order

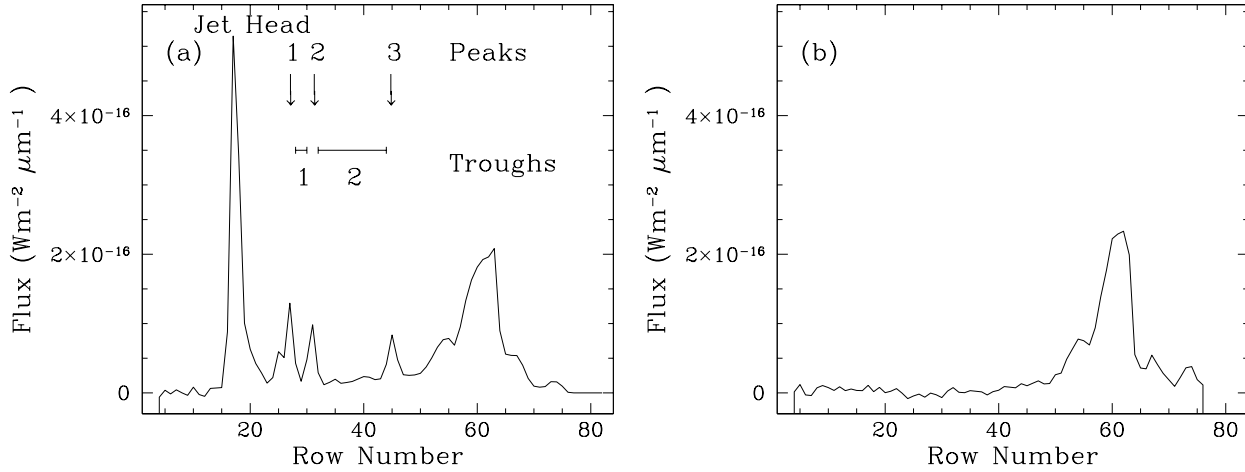


Fig. 3. **a** Cut along the jet axis in the 1–0S(1) line. Arrows mark the emission peaks, and lines mark the emission troughs. The head of the jet peaks at row 20. **b** Cut along the jet axis in a line free part of the spectrum. Emission is seen only from the nebulosity.

of magnitude less bright than the emission from the knot peaks, but it is present at all positions in the jet.

From the long slit observations, the length and width of the jet can be estimated, assuming a distance of 200 pc to the L483 system. The jet is 14400 AU long, from the start of the nebulosity, near the source, to the head of the jet. From Slit 1, which goes through the centre of the head of the jet, this has a width of 1400 AU. Slit 3 is placed 2'' below Slit 2, and, from the observations, is still placed within the jet. Assuming that the jet is symmetric about its axis, this gives a minimum width to the jet body of 400 AU.

4. Analysis

Table 2 gives intensities and column densities for each line at the head of the jet from slit 2. To calculate the intensities, the emission lines were fitted with single Gaussians, with uncertainties from a least squares fit. The line column densities can be calculated from (Gredel 1994):

$$I(\nu, J) = \frac{hc}{4\pi\lambda} A(\nu, J) N(\nu, J) \quad (1)$$

where $I(\nu, J)$ is the specific intensity of the line, $A(\nu, J)$ is the Einstein A coefficient of the transition, λ is the wavelength of the transition, and $N(\nu, J)$ is the population of the upper level.

A reliable estimate of the excitation temperature for molecules undergoing rotational and vibrational transitions can be obtained from the rotation diagram. This method can be applied if the lines are optically thin and the level populations are characterised by a single rotation temperature.

The total H_2 column density can then be calculated (Gredel 1994), using coefficients taken from Irwin (1987) for the partition function of H_2 :

$$\ln\left(\frac{N_j}{g_j}\right) = \ln\left(\frac{N_{\text{tot}}}{Z_{T_{\text{rot}}}}\right) - \left(\frac{E_u}{kT_{\text{rot}}}\right) \quad (2)$$

where N_j is the population of the upper level, g_j is the statistical weight for the transition, N_{tot} is the total H_2 column density, Z

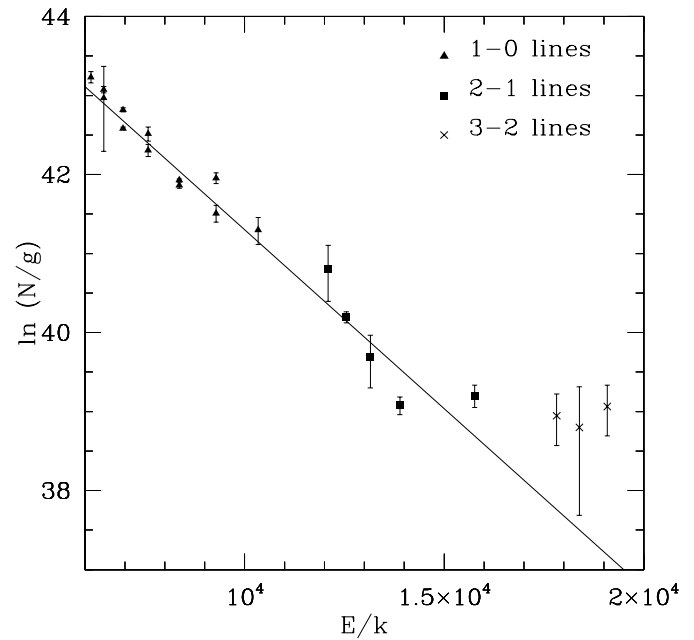


Fig. 4. Rotation diagram for the head of the jet. The gradient gives a temperature of 2200 K. The y intercept gives a hydrogen column density of 10^{17} cm^{-2} .

is the H_2 partition function, E_u is the energy of the upper level and T_{rot} is the rotation temperature.

The rotation diagram for the jet head is shown in Fig. 4. The error bars are from the uncertainties in the line integrated intensities. A straight line fit to the rotation diagram at the head of the jet, gives a rotational temperature of 2200 K from the gradient, and a total H_2 column density of $1.10 \times 10^{17} \text{ cm}^{-2}$, from the y intercept and the hydrogen partition function. This fit is shown in Fig. 4. The single rotation temperature fit, shown in Fig. 4, does not produce a good fit to the $v=2-1$ or $v=3-2$ lines. From the diagram, it is possible to see that the $v=2-1$ lines may be fit with a shallower slope, which is indicative of a higher temperature. Rotation diagrams for individual sets of lines with

Table 2. H₂ intensities and column densities for the bow shock. Numbers in brackets are the associated uncertainties

Line	λ_{rest} μm	Intensity $\times 10^{-4} \text{ erg s}^{-1} \text{ cm}^{-2} \text{ str}^{-1}$	Column density in line $\times 10^{15} \text{ cm}^{-2}$	Energy K
1-0S(0)	2.2235	0.457 (0.018)	2.548 (0.04)	6471
1-0S(1)	2.1218	1.688 (0.027)	6.544 (0.02)	6956
1-0S(2)	2.0338	0.656 (0.050)	2.128 (0.07)	7584
1-0S(3)	1.9576	1.812 (0.025)	5.352 (0.01)	8365
1-0S(4)	1.8920	0.753 (0.052)	2.162 (0.07)	9286
1-0Q(1)	2.4066	1.515 (0.011)	5.374 (0.07)	6149
1-0Q(2)	2.4134	0.455 (0.224)	2.293 (0.40)	6471
1-0Q(3)	2.4237	1.503 (0.038)	8.281 (0.03)	6956
1-0Q(4)	2.4375	0.451 (0.041)	2.624 (0.09)	7586
1-0Q(5)	2.4548	8.232 (0.031)	5.008 (0.04)	8365
1-0Q(6)	2.4756	0.216 (0.023)	1.381 (0.10)	9286
1-0Q(7)	2.5001	5.757 (0.097)	3.887 (0.16)	10341
2-1S(0)	2.3556	0.065 (0.022)	0.264 (0.29)	12095
2-1S(1)	2.2477	0.210 (0.015)	0.601 (0.07)	12550
2-1S(2)	2.1542	0.063 (0.020)	0.154 (0.28)	13150
2-1S(3)	2.0735	0.135 (0.038)	0.309 (0.10)	13890
2-1S(5)	1.9449	0.195 (0.027)	0.477 (0.13)	15763
3-2S(1)	2.3864	0.058 (0.018)	0.172 (0.27)	17818
3-2S(2)	2.2870	0.024 (0.017)	0.063 (0.51)	18386
3-2S(3)	2.2024	0.123 (0.038)	0.304 (0.27)	19086

the same v at the head of the jet were plotted, to test whether a single rotation temperature is appropriate in this case. The results are summarised in Table 3. The $v=1-0$ lines dominate the rotation diagram, as they are more numerous, and have less uncertainty associated with them due to their relative strength. The Q lines, which could be affected by the atmospheric variation at the edge of the window, do not significantly affect the calculated temperature. The $v=2-1$ lines indicate a higher rotation temperature of between 2300 K and 2900 K. The $v=3-2$ lines are very weak, and the uncertainties are such that the fit to these lines only is unconstrained and no reliable rotation temperature can be calculated. However a temperature of 3800 K can be calculated from the combined 2-1 and 3-2 lines. The higher temperatures derived from the higher energy lines are indicative of either a higher temperature component or perhaps non-LTE processes, possibly due to the differential streaming in ambipolar diffusion (O'Brien & Drury 1996), becoming significant for the population levels in the higher energy lines. UV fluorescence would also take the population levels out of LTE, but would produce stronger emission from lines with higher v , which is not observed.

Similar calculations have been carried out for several positions along the length of the jet. Due to the drop in intensity along the length of the jet, it is the 1-0 lines which dominate these calculations, although all detected lines are included. Table 4 gives the total H₂ column densities and temperatures found from slit 2, along the length of the jet. The intensity from each line was summed across a number of rows, corresponding to the size of the peaks and troughs. Nearer to the source, the line intensities become weaker and the temperatures and column densities become correspondingly more uncertain. These results are shown graphically in Fig. 5, which also shows the confidence limits on

Table 3. Temperatures at the head of the jet for differing sets of v

Lines	T _{ex} K	Uncertainty K
All lines	2200	30
1-0 only	1950	40
1-0 only, excluding Q lines	2110	60
1-0 only, Q lines only	1690	70
2-1 only	2570	310
2-1 and 3-2	3800	460

the derived parameters. This figure shows that there is probably a difference in temperature between the peaks and the troughs. The jet head, while having a similar temperature to the peaks, has a much higher column density.

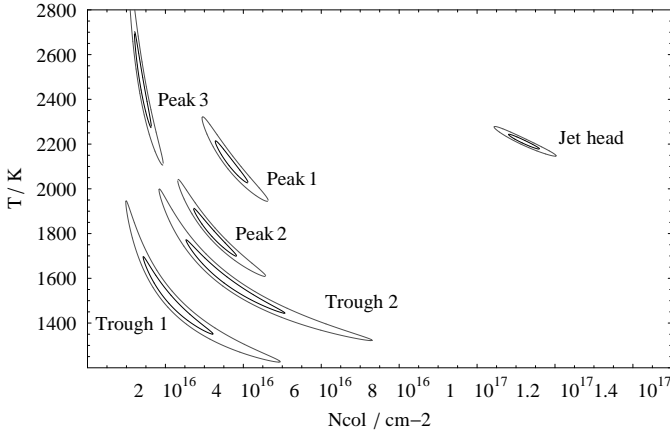
5. Shocks in the L483 protostellar jet

5.1. H₂ excitation in shocks

H₂ can be excited into emission by shock waves generated by the supersonic injection of mass into the ambient medium by the protostellar jet (Draine & McKee, 1993; Hollenbach 1997; Eisloffel, 1997). A bow shock accelerates gas ahead of the jet, and a second shock, the Mach disk, decelerates material in the jet. The bow shock is formed as shocked gas impacts the quiescent ambient material. The Mach disk is formed where the jet impacts previously shocked material. Since the ratios of the emission lines of H₂ are dependent upon the excitation mechanism, this molecule can be used as a diagnostic of the processes happening within the jet (e.g. Hartigan et al. 1996; Burton 1992; Gredel 1996).

Table 4. Temperature and total H₂ column densities along the jet from slit 2. Refer to Fig. 3 for the position.

Position (row number)	Description (see Fig. 4)	T _{ex} K	Uncertainty K	N _{H₂} x10 ¹⁷ cm ⁻²	Uncertainty x10 ¹⁷ cm ⁻²
18–21	Jet Head	2210	30	1.10	0.06
28–30	Peak 1	2120	90	0.36	0.06
30–32	Trough 1	1590	160	0.37	0.17
32–34	Peak 2	1800	110	0.32	0.07
34–46	Trough 2	1500	170	0.21	0.11
46–48	Peak 3	2470	210	0.15	0.04

**Fig. 5.** Confidence regions on temperature and column density from rotation diagram fits at various positions along the slit. Confidence levels are 1 σ (heavy) and 3 σ (light).

In the L483 jet, the emission lines observed at the jet head fall off in strength with increasing v , the $v=1-0$ lines being the strongest, and the $v=3-2$ lines much weaker. This is indicative of shock excited H₂. Processes such as UV fluorescence or H₂ reformation should produce stronger emission from higher v levels (Burton 1992).

H₂ can be excited into emission in two types of shock. A jump, or J-shock takes place where the magnetic field is weak, and the gas properties change suddenly. The bulk motion is dissipated into thermal energy, and the front is followed by a distinct region of cooling. A bow shock may consist of J shocks of decreasing strength with increasing distance from the jet axis. H₂ emission arises from the hot gas inside the wings of the bow shock and Mach disk, where the shock velocity is below the H₂ dissociation velocity (Hartigan et al. 1996). H₂ line emission and molecule dissociation controls the cooling, and the degree of dissociation is dependent upon the shock driving pressure.

In the presence of a strong magnetic field, a continuous, or C-shock takes place. This is a magnetically mediated two fluid shock. The ions are pushed ahead of the shock, and gradually heat and accelerate the predominantly neutral pre-shock material. Planar C-shocks produce a narrow range of H₂ excitation temperatures, whereas for bow C-shocks, the excitation temperature varies along the bow. For both types of shock, the molecules can be dissociated at the tip of the bow shock, where the shock velocity is at a maximum. H₂ emission arises along

the wings of the bow shock, where the effective shock velocity is lower. C-shocks produce higher column densities of shocked molecular hydrogen than J-shocks (Smith 1995).

In a slightly weaker magnetic field, a magnetic precursor can form ahead of the shock. Some ions are still accelerated, but are unable to heat the pre-shock material enough to cushion the following shock. In this case, a C-shock forms, and is followed by a J-shock, where the molecules are dissociated. H₂ emission should occur everywhere along the bow shock where the precursor exists (Hartigan et al. 1996).

5.2. Shock analysis at the jet head

The relative strengths of the strongest lines in the spectra can be compared to models of shocks in molecular jets and outflows (e.g. Smith 1995), and give an indication of the type and speed of the shock. A comparison of the L483 shock ratios with the models of Smith (1995) is given in Table 5.

The $\frac{1-0S(1)}{2-1S(1)}$ ratio indicates that either a fast C-shock with speed 40–45 km s⁻¹, or a slow J-shock, with speed 9–11 km s⁻¹, is consistent with the data. The $\frac{1-0S(3)}{2-1S(3)}$ ratio is indicative of a fast C-shock with speed ≥ 35 km s⁻¹. The value of these shock ratios suggest that the L483 outflow has a leading bow C-shock, where the jet is impacting the ambient medium with a shock speed of 40–45 km s⁻¹. In addition, the curvature in the rotation diagram suggests that the rotation temperature increases with the energy of the vibrational level. This suggests that the leading shock is a bow C-shock (Smith et al. 1991), where different speeds along the bow surface leads to different temperature regions along the bow, and so different excitation regions.

The shock speeds are not constrained by any shift in the wavelength of the H₂ lines, which were measured only at low velocity resolution. We calculate a 3 σ upper limit of 135 km s⁻¹ on the H₂ lines' velocity shifts relative to the rest velocity of the source (Sect. 2); however, this is a limit on the line-of-sight component, whereas in L483 it is clear that the outflow axis is nearly in the plane of the sky (Hatchell et al. 1999), so the velocity would be expected to be dominated by the component perpendicular to the line of sight.

Models (e.g. Hartigan 1989) of Mach disks from stellar jets indicate that the distance between the bow shock and the Mach disk is approximately 500 AU in most cases. As the emission from the bow shock in the L483 jet extends spatially across over

Table 5. Comparison of line ratios for different types of shocks, with varying speeds (Smith 1995). The type of shock is indicated by the letter, and the speed, in km s^{-1} , is then given. These are compared to the line ratios for different positions along the jet.

Ratio	Observed values in L483							Models								
	Bow	Peaks		Troughs			C-Shock speeds			J-Shock speeds						
		1	2	1	2	3	35	40	45	50	8	9	11.5	15	18.5	
$\frac{1-0S(1)}{2-1S(1)}$	8	7	9	8	6	6	47.8	20.1	10.9	5.82	4.75	17.9	10.0	4.77	4.19	3.95
$\frac{1-0S(3)}{2-1S(3)}$	13							19.28							3.93	

700 AU along the jet, we are unable to discern whether we are seeing emission from the bow shock, Mach disk, or both.

5.3. Shock velocity limit from CO observations

A strict lower limit on the shock speed can be derived from the low velocity CO outflow that surrounds the shocked H_2 jet in L483 (Hatchell et al. 1999). In a simple bow shock model, material heated by the bow shock expands sideways, sweeping up the ambient medium to create a CO shell. In the time it has taken the bow shock to travel a distance Δz along the jet axis to its current position (marked by shocked H_2) from a given position in the CO outflow, the outflow has expanded to a radius r at a velocity greater than the observed transverse expansion velocity v_\perp (as the shell expansion slows as more material is swept up). From the CO observations, both r and v_\perp can be estimated and we can use this to put a lower limit on the speed at which the bow shock progresses, v_S .

$$v_S \gtrsim \frac{\Delta z (v_R + v_B)}{2r \cos^2 i} \quad (3)$$

where v_R and v_B are the observed maximum red and blue velocities at a position Δz from the bow shock. For unknown inclination, a strict lower limit on v_S can be found by putting $\cos i = 1$. Using the values $\Delta z = 30''$ and $2r \lesssim 10''$, $v_R \simeq 3.5 \text{ km s}^{-1}$ and $v_B \simeq 6.5 \text{ km s}^{-1}$ (Hatchell et al. 1999, Figs. 7 and 9) the lower limit on the shock velocity is $v_S > 30 \text{ km s}^{-1}$. This is a strict lower limit: firstly because of the inclination angle; secondly because the measured v_\perp at Δz from the bow shock actually corresponds to an annulus of gas that was ejected further from the bow shock and thus has a greater r , a slower v_\perp and a longer travel time than the annulus ejected from Δz ; and thirdly because we are measuring the average shock speed over Δz whereas the shock will travel faster into the lower ambient density further from the star. This lower limit of 30 km s^{-1} rules out slow J shocks of $9\text{--}11 \text{ km s}^{-1}$ as the excitation mechanism.

5.4. Jet density

By considering the transfer of momentum, the ratio of the ambient to jet volume densities can be calculated by balancing the ram pressures in the jet and in the swept up ambient medium (Blondin et al. 1990):

$$v_j = v_s \left(1 + \sqrt{\frac{\rho_a}{\rho_j}} \right). \quad (4)$$

where v_j and v_s are the jet and shock velocities, respectively, and ρ_a and ρ_j are the ambient and jet densities, respectively. For the bow shock speed of 40 km s^{-1} estimated from the line ratios, and assuming a typical jet speed of 200 km s^{-1} , this gives a $\frac{\rho_a}{\rho_j}$ ratio of 16. If the jet speed were faster, then this ratio would increase. This suggests that the L483 outflow contains a light jet, which is at least a factor of 10 less dense than the medium into which it is moving.

5.5. Shock analysis at other positions

The $\frac{1-0S(1)}{2-1S(1)}$ ratios along the jet vary within the range of 6 and 9, consistent with a fast C-shock of speed $40\text{--}45 \text{ km s}^{-1}$. However, for positions away from the jet head, these ratios may indicate a slower J-shock, with speed $\leq 11 \text{ km s}^{-1}$. The lower limit to the shock speed found from the CO observations does not apply at these positions, only at the jet head. This implies that the jet could contain a series of internal shocks (Raga & Noriega-Crespo 1992). Fig. 5 suggests that the peaks have a similar temperature, but a lower column density than the jet head, which would support this case. However, there are alternative processes which could produce this pattern of temperatures and column densities. These are explored below.

One possibility is a wandering jet. Some jets have been observed to vary slightly in direction as they propagate from the central object. This could lead to apparent clumps of emission in longslit spectra, as the jet moves in and out of the slit position. However, in this case, we have two parallel slit positions, on and off the jet axis, which show the clumps at the same positions. Also the H_2 image of Fuller et al. (1995) shows that there are clumps in the jet. Therefore, the knots in the spectra of the L483 jet are not due to a wandering jet.

It is possible that the emission peaks are clumps of denser material within the jet (Burton 1992; Richter et al. 1995; Micono et al. 1998). Clumps of emission could be formed locally from ambient molecular gas though hydrodynamic instabilities in the jet flow, such as Kelvin-Helmholtz instabilities. The radiative jets entering cool molecular clouds sweep up molecular gas. The instabilities at the boundary leads to ambient material being dragged into the jet, forming dense clumps. Although the H_2 cooling timescale is < 1 year, an energetic jet could reproduce H_2 clumps at the high excitation temperatures near 2000 K. It is conceivable that these clumps would be produced at similar positions, so that the H_2 maps taken at different times will show a similar spatial distribution of knots (compare Fig. 1, taken in

1995 and Fig. 3a, taken in 1997). It is therefore possible that the clumps are formed through jet instabilities.

An alternative model suggests a continuous jet with sporadic periods of higher or episodic activity (Suttner et al. 1997; Bell 1998), possibly corresponding to some type of FU Ori object outburst. FU Ori objects are T Tauri stars that show a sudden and persistent increase in magnitude. Typically, these outbursts last for between 10 and 100 yr, with between 500 and 10000 yr between outbursts. They are thought to be due to enhanced accretion from the disk. The duration of each outburst for the L483 source implied by the size of the knots, assuming a typical jet speed of 200 km s^{-1} , is $\sim 11 \text{ yr}$, which is in line with the models. However, the inferred time between outbursts in L483 is $\sim 50 \text{ yr}$, which is an order of magnitude too short. As the driving source in L483 is thought to be an extremely young class 0 object, it is possible that the outbursts are more frequent during this early epoch.

Based on these observations, and current models of protostellar jets, it is not possible to distinguish between these possibilities. If the knots are due to intrinsic jet variabilities, then observations of the counter-jet could confirm this alternative, as the counter-jet would be expected to show the same pattern of knots, as does HH212 (Zinnecker et al. 1997). In many other sources, knots as traced by CO bullets are in pairs, which suggest intrinsic variation processes. In addition, proper motion observations of the jet could be undertaken. For intrinsic jet variations, we would expect more coherent proper motions, as the knots travel with the jet.

6. Continuous emission in the L483 protostellar jet

In addition to the emission clumps discussed in the last section, the L483 jet also shows continuous emission that extends along the full length of the jet. The emission lines produced in this process are over an order of magnitude less bright than the emission lines in the clumps. Although weak, emission is visible at all positions along the jet from star to bow shock. This low-level emission in the troughs may be residual emission behind the shocks at the peaks; jet edge entrainment (De Young 1986); emission from the warm, partially ionised jet; or unresolved subknots. In this section we discuss each of these alternatives.

H_2 emission in the wings of bow shocks continues for some distance behind the leading shock, but can it be sustained over a large enough range to explain the emission in the troughs? Numerical simulations (Suttner et al. 1997) suggest that the 1–0S(1) line intensity should drop by two orders of magnitude within 1400 AU of each jet shock. The models also show significant emission levels following the leading two shocks only. Yet in L483, low level emission is seen over more than 2100 AU between Peaks 2 and 3 (see Fig. 3a). Hatchell et al. (1999) model the temperature structure of the L483 outflow and conclude that the temperature should drop below 1000 K within 800 AU of the bow shock, at which point the ro-vibrational H_2 lines are no longer excited. The excitation analysis shows that temperatures remain above 1000 K for more than twice this distance.

However, the trough emission could be cooler than the peaks, as expected for bow shock wings – this is consistent with our excitation analysis (Fig. 5) though not definite.

In summary, the length over which the trough emission is sustained in Trough 2 and the fact that it lies behind the third shocked knot counts against a bow shock wing explanation for the trough emission.

The H_2 could be in the jet itself, if certain conditions are satisfied. The jet cannot be fully molecular as the cooling time for molecular hydrogen is only a few years, insufficient to produce ro-vibrational H_2 emission along the length of the outflow as the travel time in the jet is $\sim 300 \text{ years}$ for a 200 km s^{-1} jet. Fully molecular jets also conflict with the observations at optical wavelengths of atomic protostellar jets. If a small fraction $< 1\%$ of the jet were molecular then the cooling problem would be solved (as the molecular hydrogen radiates energy gained from the atomic fraction). The H_2 column densities correspond to a volume density of 20 cm^{-3} (assuming a jet diameter of 400 AU), much less than the measured $10^3\text{--}10^4 \text{ cm}^{-3}$ (Bacciotti et al. 1995), suggesting 0.2–2% of the jet is molecular hydrogen if the observed emission originates from the jet. Whether a small fraction of molecular hydrogen could survive over outflow timescales in a predominantly atomic jet remains to be determined.

Thirdly, the H_2 could be entrained from the ambient medium in a mixing layer along the edges of the jet, as suggested by De Young (1986). The observed H_2 column densities of a few $\times 10^{16} \text{ cm}^{-2}$ are consistent with the entrainment predictions of Taylor & Raga (1995). Predictions for temperatures in mixing layers range from a few $\times 10^3 \text{ K}$ (Lizano & Giovanardi 1995) to $10^4\text{--}10^5 \text{ K}$ (Cantó & Raga 1991; Taylor & Raga 1995): the observed temperatures are consistent with the lower end of this range. Entrainment models predict falling temperatures with distance from the star, but the uncertainties on our temperature estimates for the troughs are too large to test this prediction.

Whether or not entrainment is the explanation for excited H_2 along the length of the jet, it is clear that ro-vibrational H_2 traces only a small fraction of the total mass of the outflow. An upper limit on the directly detected H_2 mass can be found by assuming the column density of $1 \times 10^{17} \text{ cm}^{-2}$ measured at the bow shock extends over the entire 14400 AU outflow length with a (generous) width of 2100 AU ($10''$ at the distance of L483 - see map of Fuller et al. 1995), the total mass traced by H_2 is $10^{-6} M_{\odot}$, compared to more than $10^{-2} M_{\odot}$ traced by the CO outflow. As hot mixing layers should be well traced by the infrared H_2 transitions, it is clear that the total mass entrained in mixing layers is much less than the mass which has been swept up by the leading bow shock and cooled to form the CO outflow.

Finally, the H_2 could be from intermediate unresolved knots. This effect is seen in another outflow, HH 111, which shows both infrared and optical emission along the jet. The H_2 observations (Coppin et al. 1998) highlight knots at certain positions (labelled F, H, L) with what appears to be continuous emission in between, like the trough emission in L483. However, in the higher resolution optical HST images (Reipurth et al. 1997), the $\text{H}\alpha$ and [SII] emission breaks up into several subknots which

are not distinguished in the H_2 observations. The troughs in L483 may similarly consist of emission from unresolved sub-knots. The measured column densities are beam averaged over $1.2'' \times 1.2''$ pixels. Emission regions smaller than this are beam-diluted and have decreased column density when averaged over the pixel area. A factor of 2–4 in beam filling factor could explain the observed differences in column density between peaks and troughs, though not the differences in temperature (Fig. 5). This is suggestive of lower shock velocities, but similar column densities.

In order to distinguish between these alternatives for the continuous H_2 emission along the jet, higher resolution observations across and along the jet would be required. Observations along the jet would need sufficient resolution to resolve individual bow shocks. The observations across the jet would need sufficient resolution to resolve the jet, where we would expect to see emission, if the emission were from H_2 in the jet, or edge brightened emission if the emission were from a mixing layer along the jet.

7. Summary

We have presented data from longslit ro-vibrational spectroscopy of molecular hydrogen in the outflow from the protostellar source in L483. The jet shows a bow shock, and a series of emission knots leading back to the source. The excitation of the leading bow shock is consistent with a C-shock, with a speed of between 40 km s^{-1} and 45 km s^{-1} . Slower J-shocks can be ruled out, because of data from CO observations that gives a strict lower limit of 30 km s^{-1} to the shock velocity. The shock velocity indicates that the jet from L483 has a density of about 10 times less than the medium into which it is propagating.

The H_2 excitation in the emission clumps along the jet is consistent with shock excitation, and so the emission may be due to internal jet shocks. These shocks could be fast C-shocks, as at the jet head, or they could be much slower J-shocks, with speeds $\leq 11 \text{ km s}^{-1}$. However, other mechanisms such as jet instabilities or episodic activity cannot be ruled out.

In addition to the brighter emission clumps, molecular hydrogen emission is seen along the full length of the jet. This may be due to emission from H_2 in the jet, in which case the jet must contain a small fraction, less than a few percent, of molecular hydrogen. Alternatively, material may be being entrained in a mixing layer along the jet. If this is the case, then the H_2 observations clearly show that the total mass entrained in mixing layers is much less than the mass swept up by the leading bow shock. A third alternative is that the emission comes from unresolved sub-knots.

The H_2 in the clumps and along the jet has similar excitation temperatures; the emission along the jet is mostly distinguished by its low column density. The bow shock at the jet head has by far the greatest column density of H_2 . The higher excitation H_2 lines, which are weak and therefore only well detected at the jet head, have a higher excitation temperature than the lower energy lines suggesting the presence of a second, warmer, gas component. Increasing excitation temperature with vibrational

energy level is a feature of bow C-shock models, suggesting that the jet head is a bow C-shock.

Finally, using lines at different wavelengths which originate in the same upper state energy level, the extinction to the H_2 emitting material was estimated. An extinction of $A_v \sim 38 \text{ mag}$ is derived towards the K band reflection nebula and extinctions about a factor of three less than this towards the jet and jet head. These results indicate that the protostellar source is still very deeply embedded, consistent its inferred young age, and that the source is embedded in a centrally condensed region.

Although this source is the youngest yet studied using this technique, it shows many of the characteristics displayed in older sources. The H_2 excitation - and therefore the shock conditions - are similar to more evolved sources and the flow already shows a complex, knotty structure. The outflow-driving mechanism clearly begins very early in the star formation process.

Acknowledgements. Astronomy at UMIST is supported by PPARC. JVB would like to acknowledge the financial support of a PPARC studentship. The United Kingdom Infrared Telescope is operated by the Joint Astronomy Centre on behalf of the U.K. Particle Physics & Astronomy Research Council. The authors would like to thank UKIRT staff for their help and advice, particularly Tim Hawarden who carried out the observations in serviced mode.

References

- Bacciotti F., Chiuderi C., Oliva E., 1995, *A&A* 296, 185
 Bell R., 1998, *FU Orionis Outbursts*. In: Mannings V., Boss A., Russell S. (eds.) *Protostars & Planets IV*. University of Arizona Press, in press
 Blondin J.M., Fryxell B.A., Konigl A., 1990, *ApJ* 337, L37
 Burton M.G., 1992, *Aust. J. Phys.* 45, 663
 Cantó J., Raga A.C., 1991, *ApJ* 372, 646
 Coppin C.E.K., Davis C.J., Micono M., 1998, *MNRAS* 301, L10
 De Young D.S., 1986, *ApJ* 307, 62
 Draine B., McKee C.F., 1993, *ARA&A* 31, 373
 Eisloffel J., 1997, *Molecular Hydrogen Emission*. In: Reipurth B., Bertout C., (eds.) *Proc. IAU Symp. 182, Herbig-Haro Flows and the Birth of Stars*
 Fernandes A.J.L., Brand P.W.J.L., 1995, *MNRAS* 274, 639
 Fuller G.A., Lada E.A., Masson C.R., Myers P.C., 1995, *ApJ* 453, 760
 Gredel R., 1994, *A&A* 292, 580
 Gredel R., 1996, *A&A* 305, 582
 Hartigan P., 1989, *ApJ* 339, 987
 Hartigan P., Carpenter J.M., Dougados C., Skrutshie M.F., 1996, *AJ* 111, 1278
 Hatchell J., Fuller G.A., Ladd E.F., 1999, *A&A*, in press
 Hollenbach D.J., 1997, *The Physics of Molecular Shocks*. In: Reipurth B., Bertout C., (eds.) *Proc IAU Symp. 182, Herbig-Haro Flows and the Birth of Stars*
 Hora J.L., Latter W.B., 1994, *ApJ* 437, 281
 Irwin A.W., 1987, *A&A* 182, 348
 Königl A., 1995, *Rev. Mex. Astron. Astrofis.* 1 275
 Koornneef J., 1983, *A&AS* 51, 489
 Lizano S., Giovanardi C., 1995, *ApJ* 447, 742
 Masson C.R., Chernin L.M., 1993, *ApJ* 414, 230
 Micono M., Massaglia S., Bodo G., Rossi P., Ferrari A., 1998, *A&A* 333, 1001
 Myers P.C., Ladd E.F., 1993, *ApJ* 413, L47

- O'Brien I., Drury L.O'C., 1996, MNRAS 280, 550
Parker N.D., Padman R., Scott P.F., 1991, MNRAS 252, 442
Raga A.C., Noriega-Crespo A., 1992, Rev. Mex. Astron. Astrofis.24, 9
Reipurth B., Hartigan P., Heathcote S., Morse J., Bally J., 1997, AJ 114, 757
Richter M.J., Graham J.R., Wright G.S., 1995, ApJ 454, 277
Smith M.D., 1995, A&A 296, 789
Smith M.D., Brand P.W.J.L., Moorhouse A., 1991, MNRAS 248, 451
Suttner G., Smith M.D., Yorke H.W., Zinnecker H., 1997, A&A 318, 595
Taylor S.D., Raga A.C., 1995, A&A 296,823
Wright C.M., Drapatz S., Timmerman R., et al., 1996, A&A 315, L301
Zinnecker H., McCaughrean M., Rayner J., 1997, HH212. In: Malbet F., Castets A. (eds.) Poster Proc. IAU Symp. 182, Low Mass Star Formation - From Infall to Outflow. Kluwer, p. 198